ELSEVIER

www.elsevier.nl/locate/jorganchem

Journal of Organometallic Chemistry 607 (2000) 41–50

Journal of Organometallic Chemistry

# Peripherally-metallated porphyrins: synthesis and spectra of *meso*-$\eta^1$-palladio- and platinioporphyrins and the crystal structures of *cis*-{PtBr[10,20-diphenylporphyrinatonickel(II)-5-yl]($PPh_3$)$_2$} and *trans*-{PtBr[10,20-diphenylporphyrin-5-yl]($PPh_3$)$_2$}·0.25$CH_2Cl_2$

Dennis P. Arnold [a,*], Peter C. Healy [b], Margaret J. Hodgson [a], Michael L. Williams [b]

[a] *Centre for Instrumental and Developmental Chemistry, Queensland University of Technology, GPO Box 2434, Brisbane 4001, Australia*
[b] *School of Science, Griffith University, Nathan 4111, Australia*

Received 13 January 2000; received in revised form 11 March 2000

Dedicated to Professor Martin Bennett on the occasion of his retirement.

**Abstract**

A series of *meso*-$\eta^1$-palladio(II)- and platinio(II)porphyrins containing either monodentate Group 15 ligands ($PPh_3$, $AsPh_3$) or chelating diphosphines (dppe, dppp, dppf) has been prepared by oxidative addition of mono- and dibromo derivatives of 5,15-diphenylporphyrin ($H_2$DPP) to Pd(0) and Pt(0) precursors. The products were characterized by their $^1$H- and $^{31}$P-NMR, visible absorption, and mass spectra and the X-ray crystal structures of *trans*-[PtBr($H_2$DPP)($PPh_3$)$_2$] (**14**) (as a 0.25$CH_2Cl_2$ solvate) and *cis*-[PtBr(NiDPP)($PPh_3$)$_2$] (**15**) were determined. The structures show approximately square planar geometry about the Pt atoms, although there are distortions due to crowding of the $PPh_3$ ligands in **15**. The NiDPP ring in **15** suffers ruffling typical of peripherally-crowded Ni(II) porphyrins, the pairs of opposite *meso* carbons being displaced alternately $> \pm 0.4$ Å out of the $C_{20}N_4$ mean plane The conformations of the phenyl groups of the $PPh_3$ ligands indicate the presence of non-covalent phenyl–porphyrin $\pi-\pi$ interactions. These derivatives are the first isolated examples of peripheral organometallic porphyrins with direct transition metal to porphyrin $\sigma$-bonds, and they represent a new class of superstructured porphyrins with one or both faces of the macrocycle heavily shielded by the phenyl groups on the auxiliary ligands. 

*Keywords:* Palladium; Platinum; Porphyrins; Oxidative addition; Crystal structures

## 1. Introduction

The oxidative addition of aryl halides to M(0) phosphine complexes has been used for many years to prepare arylpalladium(II) and -platinum(II) compounds [1]. Recently, some attention has been paid to this reaction as a means of preparing interesting arylene-bridged dimetallic organometallics of the nickel triad [2]. We have been pursuing the use of Pd-catalyzed couplings for the preparation of novel porphyrin compounds since our first publication in 1993 [3]. In particular, we have used such couplings to prepare diporphyrins bridged by various conjugated and partially-conjugated unsaturated linkers [4], and have investigated the novel spectroscopic properties of electrogenerated anions of these dimers [5]. Many other research groups have been active in this area, and have employed Pd catalysis to prepare a spectacular variety of covalently-linked multi-porphyrin arrays. Couplings of the Heck, Suzuki, Sonogashira and Stille types, amongst others, have so far been used [6–10]. One particularly useful reaction is the coupling of *meso*-haloporphyrins with organotin or organozinc compounds [9,10], or with terminal alkynes [6,7]. The use of 5,15-diarylporphyrins such as 5,15-diphenylporphyrin ($H_2$DPP, **1**) in this area was pioneered by Therien's group [10], and this porphyrin is ideal for chemistry at the remaining lateral *meso* positions, since these two

* Corresponding author. Tel.: +61-7-38642482; fax: +61-7-38641804.
*E-mail address:* d.arnold@qut.edu.au (D.P. Arnold).

0022-328X/00/$ - see front matter 
PII: S0022-328X(00)00185-6

edges of the macrocycle are sterically unencumbered. In couplings of the *meso*-haloporphyrin using Pd(0) and phosphines, an essential step is the oxidative addition to form a *meso*-$\eta^1$-palladioporphyrin [10].

Until our preliminary communication [11], there were no reports of the isolation of such compounds. Indeed, characterized examples of directly-bonded *meso*-metalloporphyrins are very few in number [12,13]. Organometallic chemistry of metals coordinated at the centre of porphyrins is, of course, well established [14], and one group has studied $\eta^5$-octaethylporphyrinyl Ru(II) and Ir(III) complexes with one pyrrole ring $\pi$-coordinated to the metal moieties [15]. To initiate our research in this field, we prepared a range of derivatives of the type shown in Table 1, as an initial survey of the synthesis of this class of compounds containing Pd(II) and Pt(II). We now report in more detail on their synthesis and spectra, as well as detailing the first examples of single crystal X-ray structure determinations of $\eta^1$-platinioporphyrins. Our interest in these species is prompted, not only by their intrinsic novelty and their intermediacy (for Pd) in catalytic couplings, but also their potential applications. Currently, porphyrins are being applied in fields such as material science, supramolecular engineering, non-linear optics and biomimetic catalysis, and the marriage of porphyrins with organometallic chemistry at the periphery of the macrocycle may open new and useful avenues for both pure and applied research.

Table 1
Structures of starting materials and products

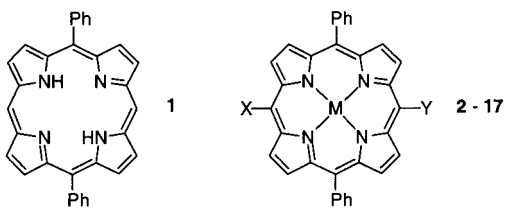


| Compound | M | X | Y |
|---|---|---|---|
| **2** | $H_2$ | H | Br |
| **3** | $H_2$ | Br | Br |
| **4** | Ni | H | Br |
| **5** | Ni | Br | Br |
| **6** | Ni | H | $PdBr(PPh_3)_2$ |
| **7** | $H_2$ | H | $PdBr(PPh_3)_2$ |
| **8** | $H_2$ | H | $Pd(AsPh_3)_2$ |
| **9** | Ni | $PdBr(PPh_3)_2$ | $PdBr(PPh_3)_2$ |
| **10** | $H_2$ | H | PdBr(dppe) |
| **11** | $H_2$ | H | PdBr(dppp) |
| **12** | $H_2$ | H | PdBr(dppf) |
| **13** | $H_2$ | H | *cis*-$PtBr(PPh_3)_2$ |
| **14** | $H_2$ | H | *trans*-$PtBr(PPh_3)_2$ |
| **15** | Ni | H | *cis*-$PtBr(PPh_3)_2$ |
| **16** | Ni | H | *trans*-$PtBr(PPh_3)_2$ |
| **17** | Ni | $PdBr(PPh_3)_2$ | *Trans*-$PtBr(PPh_3)_2$ |

## 2. Results and discussion

### 2.1. Syntheses and general properties of Pd compounds

Our interest in pursuing this chemistry stemmed from an experiment in which a Stille coupling was attempted using $Pd(PPh_3)_4$ as a catalyst. The particular reaction was very sluggish, even after extended heating. More and more catalyst was added, and eventually an impure compound possessing P-phenyl resonances in its $^1$H-NMR spectrum was isolated. This compound decomposed on standing in $CDCl_3$ solution, to form unsubstituted NiDPP. Contemplation of these facts led to the supposition that we had isolated the intermediate organopalladium(II) porphyrin. This postulate was readily confirmed by carrying out the reaction of the haloporphyrin with a stoichiometric amount of $Pd(PPh_3)_4$ in near-boiling toluene as solvent, these conditions being chosen on the basis of a previous experience of one of us (while working with Martin Bennett) with similar reactions using aryl bromides and Pt(0) [16]. The first substrate tried was NiDPPBr (**4**), and it was clear from TLC that a rapid reaction had occurred. When no further change was apparent (less than 40 min), the solvent was removed, and the glassy residue was triturated with ether to dissolve selectively the excess phosphine, leaving the organopalladiumporphyrin as a solid residue. This material exhibited $^1$H- and $^{31}$P-NMR spectra as expected for structure **6** (Table 1). This method was also used to prepare the analogous free base **7**.

In order to broaden the scope of these reactions, the universal precursor $Pd_2dba_3$ (dba = dibenzylideneacetone) was tried in combination with $PPh_3$, $AsPh_3$, and a range of bidentate diphosphines, using as substrates both **6** and **7**, as well as the nickel(II) complex (**5**) of the dibromoporphyrin (**3**). In all cases, quantitative conversion of the haloporphyrins to palladioporphyrins was demonstrated by TLC. In this initial synthetic study, in which we used very small scale preparations in most cases, we have not quantified the isolated yields of all products, nor optimized the isolations, but rather have concentrated on obtaining good characterization data. In some cases though, we were able to isolate and recrystallize the products in yields up to 65% (e.g. for **9**), with losses occurring because of the need to remove dba and excess phosphine–arsine ligands. Apart from the partial exchange of chloro for the bromo ligand (encouraged by the high *trans*-effect of the $\sigma$-bound porphyrin ligand), the compounds all survive recrystallization from dichloromethane–hexane, and also dichloromethane–methanol, provided that the precipitation is fairly rapid. Storage in solution in the presence of methanol for more than a day resulted in protolysis of the Pd–porphyrin bond, forming either $H_2$DPP or NiDPP as expected. The compounds were stable

enough in $CDCl_3$ to enable good $^1H$- and $^{31}P$-NMR spectra to be obtained. Unfortunately, these DPP derivatives are not sufficiently soluble in solvents other than dichloromethane and chloroform to enable us to obviate the chloro–bromo exchange completely. Moreover, the double oxidative addition of the *dibromo* free base **3** was unsuccessful under our conditions, because the starting material is very insoluble in toluene, even at near-boiling temperatures. We are about to embark on the use of more soluble porphyrins as a way around these problems.

For the bidentate diphosphines dppe, dppp and dppf, the reactions proceeded similarly to those for the monophosphines. The last of these ligands was recommended by Therien as being particularly active in catalysis of coupling reactions with bromoporphyrins [10]. In the preliminary communication [11], it was reported that the reaction for dppe required some 8 h heating. Reinvestigation revealed that the reaction in fact is faster than this, and is complete within 2.5 h. The fastest of these reactions is that for dppf, which accords with its good performance in coupling reactions. Reaction under the same conditions using the ligand *cis*-1,2-bis(diphenylphosphino)-ethylene led to the isolation of only the $H_2$DPP ligand, and no organopalladioporphyrin was observed. Reasons for this aberration were not addressed, but the result is consistent with the rigidity of the alkenyl chelate ring being deleterious to the oxidative addition in these rather crowded systems.

The use of Pd complexes containing the dba ligand in catalytic processes has generated some dispute in the literature, and there have been several papers addressing the exact nature of the Pd–dba species present in solution and of the complexes formed in situ by the addition of various proportions of mono- and bidentate phosphines [17]. In the present work, we were not interested in this problem per se, but rather we were concentrating on simply finding conditions which gave good yields of our porphyrin products. We found that use of a ratio porphyrin–Br:$Pd_2dba_3$ of 2:1 gave only 50% conversion of the substrate, and hence for all our experiments we used two equivalents of Pd per porphyrin, with enough Group 15 ligand to give a ratio of $>2$P(As) per Pd.

### 2.2. Syntheses and general properties of the Pt compounds

For oxidative additions to Pt(0), so far we have investigated only $PPh_3$ as a co-ligand. Thus the bromoporphyrins **2** and **4** were reacted with $Pt(PPh_3)_3$ in hot toluene, and in both cases the conversion of the starting material to Pt(II) complexes was evident by TLC almost immediately upon mixing. In each of these cases, however, it was clear that the initially-formed Pt(II) complex was being slowly converted into another product which is more mobile on TLC. By interrupting the reaction during this conversion, and isolating the products by column chromatography, we showed by NMR spectroscopy, that the first addition products are the respective *cis* isomers **13** and **15**. The final products are the *trans* isomers **14** and **16**. This isomerization is presumably assisted by the presence of the one equivalent of excess phosphine released in the addition process, since the two *cis* species are geometrically stable after removal of the excess ligand, and survive unchanged through column chromatography and slow crystallization. The geometry of these products was confirmed by crystal structure determinations of **14** and **15** (see below). In the case of the Pd(II) analogues above, the corresponding *cis* isomers were not observed. In oxidative additions of aryl halides to Ni(0), Pd(0) and Pt(0), the *trans* isomers are the usual products for all the metals [18]. The Pt(II) complexes are more stable than the Pd(II) analogues, as expected from the well-known simpler aryl organometallics.

We were also able to prepare the heterometallic bis-adduct **17** by first adding one equivalent of $Pt(PPh_3)_3$ under the usual conditions, heating for 3 h, then adding the required amounts of $Pd_2dba_3$ and $PPh_3$ to complete the Pd(0) insertion. It was clear when trying to insert a second $Pt(PPh_3)_2$ into $NiDPPBr_2$, that the second addition is much slower than the first. The $Pt(PPh_3)_2Br$ substituent appears to exert a considerable substituent effect on the porphyrin ring. This conclusion is reinforced by the fact that the derivatives **13** and **14** are stronger bases than, say, the starting material $H_2$DPPBr. During both TLC and column chromatography on silica gel, it was necessary to take the precaution of de-acidifying or adding triethylamine to the dichloromethane to prevent the formation of green protonated species. This did not seem to be necessary for the corresponding Pd complex **7**.

### 2.3. NMR spectra

The Pd complexes with monodentate Group 15 ligands, namely **6**–**9**, all exhibited sharp $^1H$-NMR spectra which were readily assignable from integration and comparison with the spectra of the starting porphyrins. Partial exchange of Cl for Br led to the observation of small peaks almost coincident with those of the bromo complexes. The phenyl groups of the $PPh_3$ and $AsPh_3$ ligands appeared upfield of the $CHCl_3$ signal, as expected for their location (on average) in the shielding zone of the magnetically anisotropic porphyrin ligand, because the L–Pd–L vector spends most time approximately orthogonal to the porphyrin plane. Clearly the rotation of the $PdL_2Br$ moiety about the Pd–porphyrin bond is slow enough on the NMR timescale at 300 MHz (and the rotations about the Pd–L and P/As–Ph bonds are fast enough), that sharp signals are observed

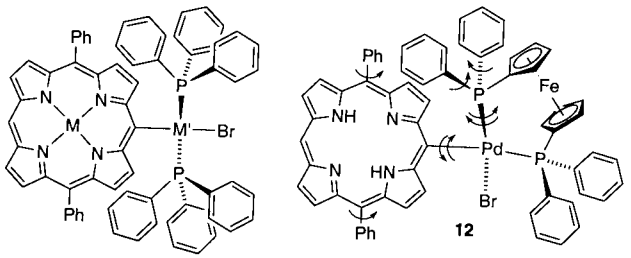


Fig. 1. Geometry of the *trans*-bis(triphenylphosphine) derivatives and the possible rotations and oscillations about the bonds in the dppf derivative **12**.

for these phenyl protons. Compared with the bromoporphyrins, small changes are apparent in the chemical shifts of the 10,20-phenyl protons, the β-pyrrole protons (which appear as usual as doublets, $J \approx 4.8$ Hz), and the remaining 15-*meso*-proton (for **6**–**8**). The $^{31}P\{^{1}H\}$ spectra of **6**, **7** and **9** exhibit singlet resonances near 30 ppm. The signals for the β-protons on carbons 3 and 7 flanking the large metallo substituent appear well downfield from the others, in the same region as the 15-*meso*-proton.

The situation is more complex for the chelating diphosphines. The proton signals for the phenyl groups overhanging the porphyrin plane shift even further upfield than for **6**–**9**, although for the dppe and dppp products **10** and **11**, the signals remain fairly sharp. However, for the ferrocenyl derivative **12**, the signals for the protons on one of the Cp rings are broad, especially the signal at 4.9 ppm and, to a lesser extent, its partner at 4.55 ppm. Moreover, the signals in the region 5–7 ppm for one pair of phenyl groups (by comparison with the rest of the series, the phenyls on the P *cis* to DPP) are extremely broad. By considering the various intramolecular motions possible for **12**, it is reasonable to assume that this behavior is due to restricted rotation(s) and/or oscillation(s) about the bonds indicated in Fig. 1, as well as within the ferrocenyl moiety. This behavior is also exhibited by one set of phenyl groups of the *cis* isomers **13** and **15** of the platinum(II) complexes. Indeed in the Ni complex **15**, the signals due to the *ortho* protons of the 10,20-phenyl groups are also broad at room temperature. We will be undertaking variable temperature studies to clarify these aspects. The X-ray crystal structure of the dppe derivative **10** was described briefly in our preliminary communication [11], and will not be discussed further here, except to note the confirmation of the fact that the phenyl groups on the *cis* phosphorus atom extend almost half-way across the porphyrin (when their positions are averaged by dppe chelate ring flipping). This is also true for the Pt derivatives **14** and **15** (see below). We propose the use of these or similar peripheral metal-centred substituents as a means of shielding the faces of the macrocycle and hence creating tailored cavities thereon [19].

The $^{31}P$ spectra of the chelated derivatives of between Pd(II) all show the expected AB spectra, with $^{2}J_{PP}$ typical for these ligands. For the *trans* Pt(II) complexes **14** and **16**, singlet $^{31}P$ resonances with $^{195}Pt$ satellites were observed, with $^{1}J_{PtP}$ values as expected for *trans* bis(phosphine) complexes (ca. 2950 Hz). This is also true for one of the $^{31}P$ resonances for the trimetallic derivative **17**. For the *cis* isomers, the widely-differing *trans*-influences of the ligands result in $^{1}J_{PtP}$ values of 4276 and 4248 Hz for P *trans* to Br and 1775 and 1795 Hz for P *trans* to DPP for **13** and **15**, respectively. Thus the *meso*-$\eta^1$-porphyrin ligand behaves on Pt(II) as a typical σ-bound hydrocarbyl group. Interestingly, for **13** the two intrinsically non-equivalent phosphorus nuclei are accidentally isochronous, but the appearance of the satellites as doublets ($^{1}J_{PP}$ 17.2 Hz) with Pt–P coupling constants as above, unambiguously determines the stereochemistry about Pt. For the Ni(II) complex **15**, the two $^{31}P$ signals differ in chemical shift by only 0.4 ppm.

Some informative trends have emerged by comparing the chemical shifts of the porphyrin protons across the present series. As usual, the β-pyrrole and *meso* protons for the Ni(II) complexes appear upfield of those for the corresponding free bases. Of more novelty are the upfield shifts of the β-pyrrole protons, and also those of the 10,20-phenyl groups, when *both* the 5- and 15-carbons are substituted with very large metal-centred substituents, (compounds **9** and **17**). This may be due to out-of-plane distortion of the porphyrin macrocycle (saddling or ruffling) [20].

### 2.4. Mass and UV–vis absorption spectra

All the complexes in the series except for the dppp complex **11** gave molecular ions (or protonated molecular ions for those containing $H_2$DPP) in FAB mass spectra. Because of the use of dichloromethane as a solvent for introducing the compounds into the matrix, the molecular ions of the chloro complexes were also observed in the case of the Pd derivatives (including the trimetallic complex **17**). This phenomenon was also observed for the free base Pt derivatives **13** and **15**, but not for **14** and **16**. Additionally, ions with $m/z$ appropriate for $(M + HCl)^+$ or $(M + HCl + H)^+$ were observed for **13** and **15**. Fragmentation was also apparent, and logical losses could be easily recognized. For example, although **11** did not exhibit a molecular ion, the fragments [Pd(dppp)Br], [Pd(dppp)] and $H_2$DPP were observed, as well as the dimer $[Pd(dppp)Br]_2$. The similar compound **10** gave only a very weak molecular ion cluster. The laser desorption technique (with or without matrix) did not allow the observation of any molecular ions, but unusually for this technique, extensive fragmentation was apparent.

The visible absorption spectra were typical for DPP derivatives. The wavelengths of the principal visible absorption bands for all the complexes and their precursors are collected in Table 2. Several trends are apparent, even in this limited set of data. All groups other than H in the 5- or 5- and 15-positions cause a red-shift for both the free bases and central metal complexes, and such shifts are typical of DPP systems [6,10]. The spectra are sensitive to the steric demands of the *meso* substituents, as seen by comparison between the dppe complex **10**, and the similar chelated derivatives **11** and **12**, and also between the *cis* and *trans* isomers of the Pt derivatives. Moreover, for the doubly-substituted complex **9**, there is a significant red-shift of all bands with respect to its monosubstituted analogue **7**, amounting to 1000 $cm^{-1}$ for the Soret bands. Perhaps this is another sign of non-planar distortion of the porphyrin [20], as suggested above in the discussion of its $^1$H-NMR spectrum. The effects of the same ligand set and geometry for Pd and Pt substituents were essentially identical, e.g. compare **6** and **16**. With regard to the substituent effects, note also that the $Pt(PPh_3)_2Br$ group did have a base-strengthening effect (see above), perhaps indicating a strong σ-inductive influence, with little π-interaction between the porphyrin and metal orbitals. It will be interesting to see whether the fluorescence emission of free base DPP is quenched by the presence of the heavy metal at the *meso* carbon in **7**, **8** etc. These studies are planned in the near future.

Table 2
Wavelengths for the principal UV–vis absorption bands for the *meso*-metalloporphyrins and their precursors (in $CH_2Cl_2$ solutions)

| | $\lambda_{max}$ (nm) | | | | |
|---|---|---|---|---|---|
| | Soret | IV | III | II | I |
| *Free bases* | | | | | |
| **1** | 405 | 502 | 535 | 575 | 630 |
| **2** | 420 | 510 | 545 | 587 | 642 |
| **3** | 421 | 520 | 555 | 600 | 658 |
| **7** | 418 | 514 | 550 | 587 | 642 |
| **8** | 416 | 513 | 548 | 586 | 641 |
| **10** | 414 | 509 | 544 | 580 | 634 |
| **11** | 426 | 520 | 557 | 592 | 647 |
| **12** | 426 | 521 | 558 | 594 | 649 |
| **13** | 430 | 523 | 559 | 590 | 650 |
| **14** | 434 | 526 | 563 | 599 | 655 |
| *Ni complexes* | | | | | |
| | Soret | | Q(1,0) | Q(0,0) | |
| NiDPP | 399 | | 514 | 547 | |
| **4** | 409 | | 523 | 555sh | |
| **5** | 419 | | 533 | vw sh | |
| **6** | 414 | | 522 | 553 | |
| **9** | 432 | | 538 | 579 | |
| **15** | 424 | | 533 | 579sh | |
| **16** | 415 | | 523 | 555sh | |

### 2.5. Crystal structures of **14** and **15**

#### 2.5.1. Trans-[PtBr($H_2$DPP)($PPh_3$)$_2$] (**14**)

The single crystal X-ray structure determination of this complex shows the molecule crystallizes as discrete monomers, with two independent molecules in the asymmetric unit and a co-crystallized molecule of dichloromethane with 50% occupancy located midway between the two molecules. The structural arrangement of these three molecules is shown in Fig. 2. Relevant geometric parameters are listed in Table 3. For both molecules, the porphyrin macrocycle is essentially planar (maximum deviations from the $C_{20}N_4$ mean plane = 0.15, 0.15 Å). The substituent phenyl groups lie at dihedral angles to the macrocycle mean plane of 56.8, 71.2° for molecule 1 and 66.3, 93.2° for molecule 2. The two *trans* $PPh_3$ ligands adopt approximately $C_3$ conformations of opposite chirality and are related by a pseudo-mirror plane of symmetry with torsion angles Pt–P(n)–C(nml)–C(nm2): −61(1), −21(1), −39(1); 79(1), 19(1), 45(1)° for molecule 1 and 74(1), 28(1), 36(1); −80(1), −31(1), −32(1)° for molecule 2. Rings 1 on both ligands in both molecules overhang the porphyrin ring in face-to face contact with the first pyrrole ring. The overall conformational structures of the two molecules are significantly different with the Br–Pt–C axis lying in the plane of the porphyrin macrocycle in molecule 1, while for molecule 2, this axis is significantly bent out of the plane (Fig. 2).

The Pt–Br distances of 2.518(1) and 2.511(1) Å are marginally longer than the distance of 2.4887(7) Å recorded for the *cis* nickel complex **15** (see below), reflecting the different *trans* influence of the $PPh_3$ ligand versus the C donor of the porphyrin ring. The Pt–C bond length of 2.05(1) Å for molecule 1 is 0.1 Å longer than the corresponding distance of 1.95 (1) Å observed for molecule 2. The reasons for this quite remarkable difference are not immediately apparent, but may be a reflection of differences in the strength of the phenyl–pyrrole π–π interactions in the two molecules. Typical Pt–C bond lengths involving non-cyclometallated $sp^2$ carbons are between 1.99 and 2.10 Å.

#### 2.5.2. Cis-[PtBr(NiDPP)($PPh_3$)$_2$] (**15**)

The single-crystal X-ray structure determination of **15** shows it to crystallize as discrete neutral molecules separated by normal van der Waals distances. A representative view of the molecular structure is shown in Fig. 3 and selected geometric parameters are listed in Table 3. The 10,20-phenyl substituents lie at dihedral angles to the macrocycle mean plane of 78.8 and 108.6°. As for the complex **14** above, these values are unremarkable for *meso*-aryl substituents, e.g. in DPP or *meso*-tetraarylporphyrins [6]. The $NiN_4$ geometry is essentially square planar with Ni–N distances ranging from 1.914(6) to 1.924(5) Å and *cis* N–Ni–N angles

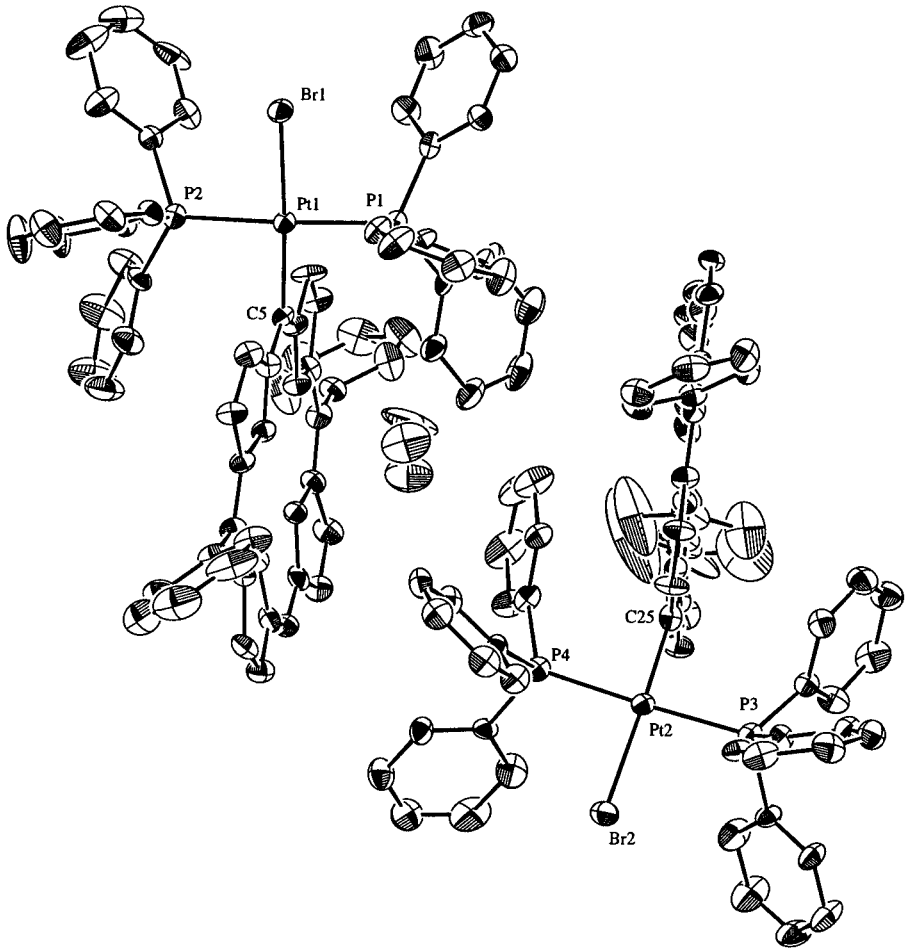


Fig. 2. Molecular structure of *trans*-[PtBr($H_2$DPP)($PPh_3$)$_2$] (**14**), showing the dispositions of molecules A and B and the dichloromethane solvent molecule, with hydrogen atoms omitted for clarity.

ranging from 89.1(2) to 90.6(2)°. As is well known for many Ni(II) porphyrin structures [20], the porphyrin ring is not planar, but rather adopts the ruffled shape, with C(10) and C(20) 0.4–0.6 Å above and C(5) and C(15) 0.4–0.6 Å below the mean $C_{20}N_4$ plane. The porphyrin ring is symmetrically coordinated to the platinum through the C(5) *meso* carbon, with Pt–C(5)–C(4,6) angles of 118.8(4) and 119.9(4)°, respectively. The Pt–C(5) bond length of 2.058(5) Å is similar to that of the longer of the two values for the structure of **14** described above.

In the triphenylphosphine ligands, the conformations of the two ligands differ significantly. Ligand 2 (*trans* to C) approximates C3 symmetry [Pt–P(n)–C(nml)–C(nm2) torsion angles: 48.1(5), 60.1(6) and 32.2(6)°], while in ligand 1, the torsion angle in phenyl group 1 increases to 80.2(5)° and in rings 2 and 3 decreases to 17.0(6) and 20.4(6)°, respectively. Fig. 3 shows that the conformation adopted by ring 1 in this ligand is likely to be a consequence of face-to-face π–π non-covalent interactions between the phenyl ring and the pyrrole

Table 3
Selected bond lengths (Å) and bond angles (°) for the complexes *trans*-{PtBr[10,20-diphenylporphyrin-5-yl]($PPh_3$)$_2$}·0.25$CH_2Cl_2$ (**14**) and *cis*-{PtBr[10,20-diphenylporphyrinatonickel(II)-5-yl]($PPh_3$)$_2$] (**15**)

| | **14** | | **15** |
|---|---|---|---|
| | Molecule A | Molecule B [a] | |
| *Bond length* | | | |
| Pt–Br | 2.518(1) | 2.511(1) | 2.4887(7) |
| Pt–P(1) | 2.323(3) | 2.309(3) | 2.248(2) |
| Pt–P(2) | 2.307(3) | 2.325(3) | 2.381(2) |
| R–C(5) | 2.05(1) | 1.95(1) | 2.058(5) |
| *Bond angle* | | | |
| Br–Pt–P(1) | 89.52(8) | 91.80(9) | 171.08(4) |
| Br–Pt–P(2) | 88.88(8) | 91.12(9) | 87.93(4) |
| Br–Pt–C(5) | 175.0(3) | 177.2(3) | 83.1(2) |
| P(1)–Pt–P(2) | 176.2(1) | 176.8(1) | 100.94(6) |
| P(1)–Pt–C(5) | 92.6(3) | 89.9(3) | 88.0(2) |
| P(2)–Pt–C(5) | 89.2(3) | 87.3(3) | 170.8(2) |

[a] For molecule B, read Pt = Pt(2), P(1) = P(3), P(2) = P(4), Br = Br(2), C(5) = C(25) (see Fig. 2).

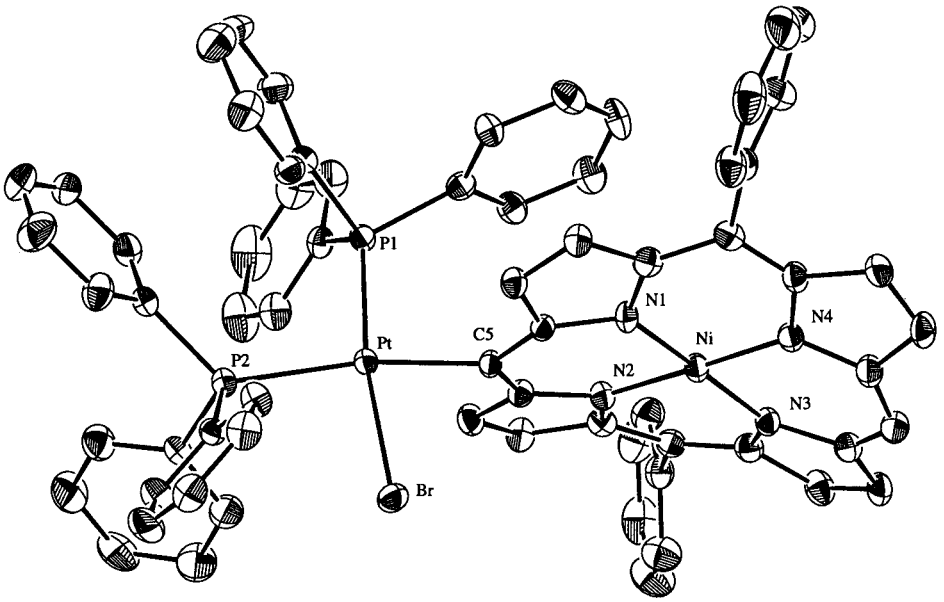


Fig. 3. Molecular structure of *cis*-[PtBr(NiDPP)($PPh_3$)$_2$] (**15**), with hydrogen atoms omitted for clarity.

moiety of the macrocycle, as noted above for **14**, and also clearly seen in the published structure of Pd complex **10** [11]. The crowding between the two bulky $PPh_3$ ligands is reflected in (i) the increase in the P–Pt–P angle to 100.94(6); (ii) the unusually large Pt–P(2)–C(221) angle of 126.0(2)°; and (iii) the tetrahedral distortion of the $PtP_2CBr$ coordination geometry about the platinum atom, with P(2)–PtC(5) and P(1)–Pt–Br angles of 170.8(2) and 171.08(4)°. To this list could be added the large difference of ca. 0. 15 Å between the Pt–P(1) and Pt–P(2) bond lengths, although some of this is no doubt due to the widely-differing *trans* influences of the ligands Br and σ-bound C. In complex **10**, the corresponding difference in the two Pd–P bond lengths is ca. 0.09 Å [11].

## 3. Experimental

Syntheses involving zerovalent metal precursors were carried out in an atmosphere of high-purity argon using conventional Schlenk techniques, but subsequently the Pd(II) and Pt(II) products were manipulated in air. The porphyrin starting materials 5,15-diphenylporphyrin (**1**), 5-bromo-10,20-diphenylporphyrin (**2**), 5,15-dibromo-10,20-diphenylporphyrin (**3**) [10], and the respective Ni(II) complexes of the last two derivatives (**4**, **5**) [6] were prepared by literature procedures, as were the Pd(0) [21] and Pt(0) [22] precursors. All other reagents and ligands were used as received from Sigma-Aldrich. Toluene was of AR grade, stored over sodium wire, and degassed by heating and stirring at 105° under argon flow. All other solvents were of AR grade, and dichloromethane and chloroform were stored over anhydrous sodium carbonate. Analytical TLC was carried out on Merck silicagel 60 $F_{254}$ plates, and column chromatography was performed using Merck silicagel, 230–400 mesh. NMR spectra were recorded on a Varian unity 300 instrument in $CDCl_3$ solutions, except where otherwise noted, using $CHCl_3$ as the reference at 7.26 ppm for $^1H$ spectra, and external 85% $H_3PO_4$ as the reference for the proton-decoupled $^{31}P$ spectra. UV–vis spectra were recorded on a Cary 3 spectrophotometer in dichloromethane solutions. In some cases, both chloro and bromo complexes are known to be present in the products, but extinction coefficients are quoted using the molecular weight of the bromo species. Errors introduced by this will be small since the molecular weights differ by only about 4%. FAB mass spectra were recorded on a VG-ZAB instrument at the Research School of Chemistry, The Australian National University, or a Kratos Concept instrument at the Central Science Laboratory, University of Tasmania. Samples were dissolved in dichloromethane, and dispersed in a 4-nitrobenzyl alcohol matrix. In the data below, masses are given for the strongest peak in the isotope cluster. Elemental analyses were carried out by the Microanalytical Service, The University of Queensland.

### 3.1. Syntheses using $Pd(PPh_3)_4$

As an example of this method, NiDPPBr (**4**) (6.9 mg, 0.012 mmol) was added to degassed toluene (5 ml) at ca. 105° with stirring. Solid $Pd(PPh_3)_4$ (12 mg, 0.01 mmol) was added, and heating and stirring were continued. TLC (elution with 50/50 dichloromethane–hexane) showed completion of the reaction within 40 min.

The toluene was removed under vacuum, and the residue was triturated three times with ether. Each time the supernatant was decanted, then the volatiles were removed under vacuum, leaving the product PdBr(NiDPP)($PPh_3$)$_2$ (**6**) as purple microcrystals. TLC showed the absence of the starting material. As described in the text above, some exchange to form the chloro analogue occurred in the presence of chlorinated solvents. This method was also used to prepare PdBr($H_2$DPP)($PPh_3$)$_2$ (**7**).

Data for **6**: $^1$H-NMR: $\delta$ 6.6 (18H, m, PPh), 7.2 (12H, m, PPh), 7.6 (6H, m, *m*-, *p*-10,20-Ph), 7.91 (4H, dd, *o*-10,20-Ph), 8.24, 8.69, 8.94, 9.40 (each 2H, d, β-H), 9.55 (1H, s, *meso*-H); $^{31}$P-NMR: $\delta$ 29.8 (chloro complex 30.1); UV–vis: $\lambda_{max}$ ($\varepsilon/10^3$ $M^{-1}$ $cm^{-1}$) 414 (210), 484 sh (3.5), 522 (15.9), 553 sh (4.3) nm; FABMS: 1228.0 ($M^+$ Anal. Calc. 1228.10), $M^+$ for chloro complex also observed.

Data for **7**: $^1$H-NMR ($C_6D_6$): $\delta$ −2.61 (2H, br s, NH), 6.2–6.4 (18H, m, M), 7.5–7.7 (18H, m, PPh and *m*-, *p*-10,20-Ph), 8.17 (4H, dd, *o*-10,20-Ph), 8.72 (2H, d, β-H), 9.08 (4H, br s, 2 × β-H), 9.85 (1H, s, *meso*-H), 10.28 (2H, d, β-H); $^{31}$P-NMR ($C_6D_6$): $\delta$ 29.7; UV–vis: $\lambda_{max}$ ($\varepsilon/10^3$ $M^{-1}$ $cm^{-1}$) 400 sh (70.4), 418 (330), 482 (3.6), 514 (13.7), 550 (10.2), 587 (4.4), 642 (6.3) nm; FABMS: 1173.0 ($MH^+$ Anal. Calc. 1173.19), $MH^+$ for chloro complex also observed.

### 3.2. Syntheses using $Pd_2(dba)_3$ and monodentate ligands

As an example of this method, $H_2$DPPBr (**2**) (5.4 mg, 0.01 mmol) was added to degassed toluene (5 ml) at ca. 105° with stirring. Solid $AsPh_3$ (12 mg, 0.04 mmol) and then $Pd_2(dba)_3$ (9 mg, 0.01 mmol) were added, and heating and stirring were continued. TLC (elution with 50/50 dichloromethane–hexane) showed completion of the reaction within 5 min. After 20 min, the toluene was removed under vacuum, and the residue was triturated three times with ether. Each time the supernatant was decanted, then the volatiles were removed under vacuum, leaving the product PdBr($H_2$DPP)($AsPh_3$)$_2$ (**8**) as purple microcrystals. TLC showed the absence of the starting material. As described above, some exchange to form the chloro analogue occurred in the presence of chlorinated solvents. This method was also used to prepare **6**, **7**, and **9** (using doubled molar amounts of Pd(0) and $Ph_3P$ for **9**, and heating for 40 min in each case). In the case of **6** and **7**, it was shown that the reaction of all the bromoporphyrin required two equivalents of Pd, i.e. Por–Br:$Pd_2dba_3$ = 1:1.

Data for **8**: $^1$H-NMR: $\delta$ −3.41 (2H, br s, NH), 6.4 (18H, m, AsPh), 7.0 (12H, dd, AsPh), 7.7 (6H, m, *m*-, *p*-10,20-Ph), 8.11 (4H, dd, *o*-10,20-Ph), 8.41, 8.85, 9.14, 9.72 (each 2H, d, β-H), 9.85 (1H, s, *meso*-H); UV–vis: $\lambda_{max}$ ($\varepsilon/10^3$ $M^{-1}$ $cm^{-1}$) 398 sh (83.0), 416 (319), 480 (4.5), 513 (14.9), 548 (11.0), 586 (4.7), 641 (6.6) nm; FABMS: 1261.0 ($MH^+$ Anal. Calc. 1261.09), $MH^+$ for chloro complex also observed.

Data for **9**: $^1$H-NMR: $\delta$ 6.7 (36H, m, PPh), 7.2 (24H, m, PPh), 7.6 (6H, m, *m*-, *p*-10,20-Ph), 7.83 (4H, dd, *o*-10,20-Ph), 8.08, 9.29 (each 2H, d, β-H); $^{31}$P-NMR: $\delta$ 29.0; UV–vis: $\lambda_{max}$ ($\varepsilon/10^3$ $M^{-1}$ $cm^{-1}$) 432 (210), 498 (5.4), 538 (18.1), 579 (9.4) mm; FABMS: 1937.9 ($M^+$ Anal. Calc. 1938.10), $M^+$ for bromochloro and dichloro complexes also observed.

### 3.3. Syntheses using $Pd_2(dba)_3$ and bidentate diphosphines

Toluene (10 ml) was added to a Schlenk flask and heated to 105° under a stream of argon. 1,2-Bis(-diphenylphosphino)ethane (dppe, 32 mg, 0.08 mmol) was added, followed by $Pd_2dba_3$ (18 mg, 0.02 mmol). The dark purple color of the palladium starting material faded rapidly, leaving a clear yellow solution. After stirring for a further 10 min, $H_2$DPPBr (**2**) (10.8 mg, 0.02 mmol) was added, and the mixture was stirred at 105° for a further 2.5 h, and the reaction progress was monitored by TLC using dichloromethane–hexane 1:1 as the eluent. After cooling to room temperature, the volume was reduced to about one-third under vacuum, and ether was added to precipitate the product PdBr($H_2$DPP)(dppe) (**10**) as dark purple crystals (17 mg, 80%). The crystal structure of this complex was reported in our preliminary communication [11]. This method was also used to prepare **11** (heating for 4 h, 70% yield) and **12**. For **12**, the bromoporphyrin was consumed within 40 min, and the product precipitated directly from the hot reaction mixture. A 60% yield of **12** was obtained by cooling, collecting the brown powder, washing with cold toluene (2 ml), then hexane (2 ml), and vacuum drying.

Data for **10**: $^1$H-NMR: $\delta$ −2.95 (2H, br s, NH), 2.53 (4H, m, $PCH_2$), 6.24 (4H, td, *m*-PPh on P *cis* to DPP), 6.48 (4H, dd, *o*-PPh on P *cis* to DPP), 6.72 (2H, br t, *p*-PPh on P *cis* to DPP), 7.6–7.8 (12H, m, 10,20-Ph and PPh on P *trans* to DPP), 8.05 (2H, br d, PPh on P *trans* to DPP), 8.24 (2H, br d, PPh on P *trans* to DPP), 8.3–8.4 (4H, m, 10,20-Ph), 8.52, 8.87, 9.18, 9.52 (each 2H, d, β-H), 9.94 (1H, s, *meso*-H); $^{31}$P-NMR: $\delta$ 42.6 (d, $J_{PP}$ 28 Hz), 57.0 (d, $J_{PP}$ 28 Hz); UV–vis: $\lambda_{max}$ ($\varepsilon/10^3$ $M^{-1}$ $cm^{-1}$) 397 sh (108), 414 (303), 509 (12.5), 544 (7.5), 580 (5.7), 634 (5.7) nm; FABMS: 1047.1 ($MH^+$ Anal. Calc. 1047.14), $MH^+$ for chloro complex also observed.

Data for **11**: $^1$H-NMR: $\delta$ −2.95 (2H, br s, NH), 1.98 (2H, br m, $CH_2$), 2.35–2.5 (4H, br m, $PCH_2$), 5.52 (4H, td, *m*-PPh on P *cis* to DPP), 5.60 (2H, dd, *p*-PPh on P *cis* to DPP), 6.16 (4H, dd, *o*-PPh on P *cis* to DPP), 7.55–7.7 (12H, m, 10,20-Ph and PPh on P *trans* to DPP), 8.07 (2H, br d, PPh on P *trans* to DPP), 8.17 (4H, m, 10,20-Ph), 8.29 (2H, br d, PPh on P *trans* to

DPP), 8.65, 8.85, 9.15, 9.82 (each 2H, d, β-H), 9.95 (1H, s, *meso*-H); $^{31}$P-NMR: $\delta$ −1.4 (d, $J_{PP}$ 53 Hz), 21.2 d, $J_{PP}$ 53 Hz); UV–vis: $\lambda_{max}$ ($\varepsilon/10^3$ $M^{-1}$ $cm^{-1}$) 426 (324), 492 (4.0), 520 (14.6), 557 (9.8), 592 (4.8), 647 (6.2) nm.

Data for **12**: $^1$H-NMR: $\delta$ −3.25 (2H, br s, NH), 3.65 (2H, br dd, 3,4-Cp *trans* to DPP), 4.17 (2H, br, 2,5-Cp *trans* to DPP), 4.55 (2H, br, 3,4-Cp *cis* to DPP), 4.9 (2H, vbr, 2,5-Cp *cis* to DPP), ca. 5.4 (vbr, PPh on P *cis* to DPP), 6.2 (vbr, PPh on P *cis* to DPP), 7.6–7.8 (12H, m, 10,20-Ph and PPh on P *trans* to DPP), 8.11 (2H, br d, PPh on P *trans* to DPP), 8.26 (2H, br d, PPh on *P trans* to DPP), 8.48 (4H, br t, 10,20-Ph), 8.73, 8.84, 9.11, 10.00 (each 2H, d, β-H), 9.81 (1H, s, *meso*-H); $^{31}$P-NMR: $\delta$ 18.5 (d, $J_{PP}$ 34 Hz), 37.5 (d, $J_{PP}$ 34 Hz); UV–vis: $\lambda_{max}$ ($\varepsilon/10^3$ $M^{-1}$ $cm^{-1}$) 426 (324), 491 (4.4), 521 (14.9), 558 (10.8), 594 (4.9), 649 (6.5) nm; FABMS: 1203.2 ($MH^+$ Anal. Calc. 1203.2). Found: C, 66.2; H, 4.2; N, 4.8. $C_{66}H_{49}BrFeNO_2Pd$ requires C, 65.9; H, 4.1; N, 4.7%.

### 3.4. Syntheses of Pt(II) complexes

Toluene (5 ml) was added to a Schlenk flask and heated to 105° under a stream of argon. $Pt(PPh_3)_3$ (16 mg, 0.017 mmol) was added, followed by $H_2$DPPBr (9 mg, 0.017 mmol). The reaction mixture was stirred under argon and a sample was removed for TLC analysis ($CH_2Cl_2$–hexane 1:1) after 12 min. This showed the presence of the *cis* isomer **13** as the major, less mobile product, with a small amount of *trans* isomer **14**. The reaction mixture was then cooled, and the solvent was removed under vacuum. The residue was separated by column chromatography, eluting with $CH_2Cl_2$–hexane/$Et_3N$ 80:20:5. Unreacted $H_2$DPPBr was eluted first, followed by **14** then **13**. The isolated **13** was recrystallized from $CH_2Cl_2$–hexane. By extending the heating time to 6 h in a separate experiment, the *trans* isomer **14** was isolated as the major product using $CH_2Cl_2$–hexane/$Et_3N$ 70:30:1 as eluent, and was recrystallized from $CH_2Cl_2$–hexane.

This method was also used to prepare the *cis* and *trans* isomers of the products containing NiDPP, **15** and **16**, respectively.

Data for **13**: $^1$H-NMR: $\delta$ −3.2 (vbr s, NH), 6.0 (vbr, Ph on P *cis* to DPP), 6.8 (vbr, Ph on P *cis* to DPP), 7.2–7.4 (br + m, PPh), 7.7–7.9 (br + m, PPh and *m*-, *p*-10,20-Ph), 8.10, 8.31 (each 2H, br d, *o*-10,20-Ph), 8.77, 8.82, 9.10, 10.16 (each 2H, d, β-H), 9.81 ($^1$H, s, *meso*-H); $^{31}$P-NMR: $\delta$ 22.2 (s, $J_{PtP}$ *trans* to Br 4276 Hz, $J_{PtP}$ *trans* to DPP 1775 Hz, satellites each d, $J_{PP}$ 17.2 Hz); UV–vis: $\lambda_{max}$ ($\varepsilon/10^3$ $M^{-1}$ $cm^{-1}$) 430 (370), 493 (4.1), 523 (13.8), 559 (10.0), 590 (4.9), 650 (6.2) nm; FABMS: 1261.3 ($MH^+$ Anal. Calc. 1261.25).

Data for **14**: $^1$H-NMR: $\delta$ −3.32 (2H, br s, NH), 6.4 − 6.55 (18H, m, PPh), 7.2–7.3 (12H, m, PPh), 7.7 (6H, m, *m*-, *p*-10,20-Ph), 8.10 (4H, dd, *o*-10,20-Ph), 8.35, 8.80, 9.10, 9.76 (each 2H, d, β-H), 9.82 (1H, s, *meso*-H); $^{31}$P-NMR: $\delta$ 27.8 ($J_{PtP}$ 2958 Hz); UV–vis: $\lambda_{max}$ ($\varepsilon/10^3$ $M^{-1}$ $cm^{-1}$) 434 (393), 495 (4.1), 526 (13.6), 563 (11.5), 599 (4.5), 655 (7.5) nm; FABMS: 1261.3 ($HM^+$ Anal. Calc. 1261.25).

Data for **15**: $^1$H-NMR: $\delta$ 6.2 (vbr, Ph on P *cis* to DPP), 6.7 (vbr, Ph on P *cis* to DPP), 7.2–7.4 (m, PPh), 7.6–7.8 (br + m, PPh and *m*-, *p*-10,20-Ph), 8.0 (br, *o*-10,20-Ph), 8.61, 8.73, 8.92, 9.91 (each 2H, d, β-H), 9.49 (1H, s, *meso*-H); $^{31}$P-NMR: $\delta$ 22.4 (d, $J_{PP}$ 16.9 Hz, $J_{PtP}$ *trans* to Br 4248 Hz), 22.8 (d, $J_{PP}$ 16.9 Hz, $J_{PtP}$ *trans* to DPP 1795 Hz); UV–vis: $\lambda_{max}$ ($\varepsilon/10^3$ $M^{-1}$ $cm^{-1}$) 424 (183), 533 (13.0), 579 sh (2.8) nm; FABMS: 1318.3 ($M^+$ Anal. Calc. 1318.16).

Data for **16**: Found: C, 61.65; H, 3.7; N, 4.2. $C_{68}H_{49}BrN_4NiP_2Pt$ requires C, 62.0; H, 3.75; N, 4.25%. Spectroscopic data for this compound were given in our preliminary communication [11].

The mixed Pd–Pt complex **17** was prepared as follows. $NiDPPBr_2$ (**5**) (8.5 mg, 0.013 mmol) was added to degassed toluene (5 ml) at ca. 105° with stirring. Solid $Pt(PPh_3)_3$ (12.5 mg, 0.013 mmol) was added, and heating and stirring were continued. TLC showed almost complete reaction of **5** within 1 h. The conversion of the initial *cis* product to the *trans* isomer was about 50% complete after 3 h, at which time $PPh_3$ (15.8 mg, 0.06 mmol) and $Pd_2dba_3$ (12.4 mg, 0.014 mmol) were added, and heating and stirring were maintained for a further 3 h. TLC showed only one major product. The toluene was removed under vacuum, and the residue was triturated three times with ether. Each time the supernatant was decanted, then the volatiles were removed under vacuum, leaving the product (NiDPP)[$PdBr(PPh_3)_2$][$PtBr(PPh_3)_2$] (**17**) as purple microcrystals.

Data for **17**: $^1$H-NMR: $\delta$ 6.6–6.75 (36H, m, PPh), 7.1–7.3 (24H, m, PPh), 7.7 (6H, m, *m*-, *p*-10,20-Ph), 7.84 (4H, m, *o*-10,20-Ph), 8.07, 8.09, 9.29, 9.48 (each 2H, d, H); $^{31}$P-NMR: $\delta$ 27.5 (PtP, $J_{PtP}$ 2967 Hz), 28.8 (PdP); FABMS: 2026.3 ($M^+$ Anal. Calc. 2027.16), $M^+$ for monochloro complex also observed.

## 4. Crystal structure determinations

### 4.1. Data collection, structure solution and refinement

Crystals of the compounds, suitable for X-ray diffraction studies, were grown by slow diffusion of hexane into dichloromethane solutions of the complexes. Unique data sets were collected at 293 K with a Rigaku AFC7R rotating anode diffractometer ($\omega$-$2\theta$ scan mode, monochromated Mo–$K_\alpha$ radiation $\lambda = 0.7107$ Å) to $2\theta_{max} = 50\%$ yielding $N$ independent reflections, $N_0$ with $I > 2\sigma(I)$ being considered observed. Empirical

absorption correction was applied based on $\psi$-scans. The structures were solved by heavy atom Patterson techniques, expanded by using Fourier techniques and refined by full-matrix least-squares on $|F|$ using the TEXSAN crystallographic software package, version 1.8, from the Molecular Structure Corporation [23]. One molecule of dichloromethane with 50% occupancy was located in the structure of **14**. Non-hydrogen atoms were refined anisotropically; $(x, y, z, U_{iso})_H$ were included and constrained at estimated values. The hydrogen atoms on the porphyrin nitrogens in the free base were not located. Statistical weights were employed. Conventional residues, $R$, $R_w$, are quoted at convergence.

### 4.2. Crystal data

**14**: $2\{trans\text{-}[PtBr(H_2DPP)(PPh_3)_2]\}\cdot 0.5CH_2Cl_2$, $C_{136.5}H_{103}Br_2ClN_8P_4Pt_2$, $M = 2564.7$, triclinic $P\bar{1}$ (no. 2), $a = 16.735(3)$, $b = 23.358(4)$, $c = 15.119(2)$ Å, $\alpha = 95.81(2)$, $\beta = 102.41(1)$, $\gamma = 82.05(2)°$, $V = 5701$ Å$^3$, $Z = 2$, $D_{calc} = 1.49$ g cm$^{-3}$, $F(000) = 2562$, $\mu = 32.8$ cm$^{-1}$, crystal size $= 0.30 \times 0.30 \times 0.10$ mm; $T_{min,max} = 0.522, 0.720$, $N = 20\ 106$, $N_0 = 10\ 036$ ($> 2\sigma(I)$); $R = 0.046$, $R_w = 0.045$.

**15**: *cis*-$[PtBr(NiDPP)(PPh_3)_2]$, $C_{68}H_{49}BrN_4NiP_2Pt$, $M = 1317.8$, monoclinic $P2_1/n$ (no. 14 variant), $a = 17.932(4)$, $b = 10.924(6)$, $c = 27.847(6)$ Å, $\beta = 97.94(2)°$, $V = 5402$ Å$^3$, $Z = 4$, $D_{calc} = 1.62$ g cm$^{-3}$, $F(000) = 2624$, $\mu = 37.7$ cm$^{-1}$, crystal size $= 0.55 \times 0.15 \times 0.05$ mm; $T_{min,max} = 0.629, 0.828$, $N = 10\ 067$, $N_0 = 6153$ ($> 2\sigma(I)$); $R = 0.030$, $R_w = 0.028$.

## 5. Supplementary material

Crystallographic data for the structural analyses have been deposited with the Cambridge Crystallographic Data Centre, CCDC nos. 141068 and 141069. Copies of this information may be obtained free of charge from The Director, CCDC, 12 Union Road, Cambridge CB2 IEZ, UK [fax: +44-1223-336033] or e-mail: deposit@ccdc.cam.ac.uk or http://www.ccdc.cam.ac.uk.

## Acknowledgements

We thank the Australian Research Council for a Small Grant to D.P.A. and for financial support for the purchase of the diffractometer, and the Faculty of Science, Q.U.T., for a post-graduate scholarship for M.J.H.

## References

[1] See for example, J.K. Kochi, in: Organometallic Mechanisms and Catalysis, Part I, Academic, New York, 1978, (Chapter 7).
[2] (a) J. Manna, C.J. Kuehl, J.A. Whiteford, P.J. Stang, Organometallics 16 (1997) 1897. (b) Y.-J. Kim, S.-W. Song, S.-C. Lee, S.-W. Lee, K. Osakada, T. Yamamoto, J. Chem. Soc. Dalton Trans. (1998) 1775.
[3] D.P. Arnold, L.J. Nitschinsk, Tetrahedron Lett. 34 (1993) 693.
[4] D.P. Arnold, D.A. James, J. Org. Chem. 62 (1997) 3460.
[5] D.P. Arnold, G.A. Heath, D.A. James, New J. Chem. 22 (1998) 1377.
[6] D.P. Arnold, R.C. Bott, H. Eldridge, F. Elms, G. Smith, M. Zojaji, Aust. J. Chem. 50 (1997) 495.
[7] R.W. Boyle, C.K. Johnson, D. Dolphin, J. Chem. Soc. Chem. Commun. (1995) 527.
[8] See for example (a) R. Gauler, N. Risch, Eur. J. Org. Chem. (1998) 1193. (b) J.P. Strachan, S. Gentemann, J. Seth, W.A. Kalsbeck, J.S. Lindsey, D. Holten, D.C. Bocian, Inorg. Chem. 37 (1998) 1191. (c) R.W. Wagner, T.E. Johnson, F. Li, J.S. Lindsey, J. Org. Chem. 60 (1995) 5266. (d) K.S. Chan, X. Zhou, M.T. Au, C.Y. Tam, Tetrahedron 51 (1995) 3129.
[9] (a) S.G. DiMagno, V.S.-Y. Lin, M.J. Therien, J. Am. Chem. Soc. 115 (1993) 2513. (b) V.S.-Y. Lin, S.G. DiMagno, M.J. Therien, Science 264 (1994) 1105.
[10] S.G. DiMagno, V.S.-Y. Lin, M.J. Therien, J. Org. Chem. 58 (1993) 5983.
[11] D.P. Arnold, Y. Sakata, K. Sugiura, E.I. Worthington, J. Chem. Soc. Chem. Commun. (1998) 2331.
[12] K.M. Smith, K.C. Langtry, O.M. Minnetian, J. Org. Chem. 49 (1984) 4602.
[13] A.G. Hyslop, M.A. Kellett, P.M. Iovine, M.J. Therien, J. Am. Chem. Soc. 120 (1998) 12676.
[14] R. Guilard, E. Van Caemelbecke, A. Tabard, K.M. Kadish, The Porphyrin Handbook, vol. 3, Academic, London, 1999 Chapter 21.
[15] (a) K.K. Dailey, G.P.A. Yap, A.L. Rheingold, T.B. Rauchfuss, Angew. Chem. Int. Ed. Engl. 35 (1996) 1833. (b) K.K. Dailey, T.B. Rauchfuss, Polyhedron 16 (1997) 3129.
[16] D.P. Arnold, M.A. Bennett, Inorg. Chem. 23 (1984) 2117.
[17] See for example (a) C. Amatore, A. Jutand, F. Khalil, M.A. M'Barki, L. Mottier, Organometallics 12 (1993) 3168. (b) C. Amatore, G. Brocker, A. Jutand, F. Khalil, J. Am. Chem. Soc. 119 (1997) 5176 and refs. therein.
[18] (a) G.W. Parshall, J. Am. Chem. Soc. 96 (1974) 2360. (b) Y.J. Kim, R. Sato, T. Maruyuma, K. Osakada, T. Yamamoto, J. Chem. Soc. Dalton Trans. (1994) 943.
[19] H. Ogoshi, T. Mizutani, Acc. Chem. Res. 31 (1998) 81.
[20] See for example (a) J.A. Shelnutt, X.-Z. Song, J.-G. Ma, S.-L. Jia, W. Jentzen, C.J. Medforth, Chem. Soc. Rev. 27 (1998) 31. (c) M.O. Senge, M.W. Renner, W.W. Kalisch, J. Fajer, J. Chem. Soc. Dalton Trans. (2000) 381.
[21] D.R. Coulson, Inorg. Synth. 28 (1990) 107.
[22] R. Ugo, F. Cariati, G. La Monica, Inorg. Synth. 28 (1990) 123.
[23] TEXSAN, Single Crystal Structure Analysis Software, version 1.8, Molecular Structure Corporation, Woodlands, TX, 1997.